Appearance of target pattern and spiral flames in radial microchannels with CH_4-air mixtures

Sudarshan Kumar,[1] Kaoru Maruta,[2] S. Minaev,[3] and R. Fursenko[3]
[1]*Department of Aerospace Engineering, Indian Institute of Technology Bombay, Powai, Mumbai, 400 076 India*
[2]*Institute of Fluid Science, Tohoku University, 2-1-1 Katahira Aoba-ku Sendai, 980-8577 Japan*
[3]*Institute of Theoretical and Applied Mechanics, SB-RAS, Novosibirsk, Russia*

(Received 26 August 2007; accepted 19 December 2007; published online 4 February 2008)

This paper presents the experimental evidence of the formation of rotating spiral flames with premixed methane-air mixtures introduced at the center of the two parallel circular quartz plates which are separated by a millimeter scale distance ($\leq$5 mm). Both plates are externally heated to create a positive wall temperature gradient in the flow direction to resemble heat recirculation through solid walls, which is a requisite to obtain stabilized combustion in microburners. Contrary to the general perception of a stable premixed flame front at a radial location, a variety of nonstationary flame propagation modes are observed. For lower mixture flow rates and a range of mixture equivalence ratios, a radial flame propagation mode is observed with simultaneous presence of two circular flames at different radial locations. For higher flow rates, a rotating spiral flame propagation mode is observed. In addition to radial and spiral flame propagation modes, random and unsymmetrical flame oscillations are also observed. The rotational rates of the spiral flame fronts were observed to vary from 28 to 83 Hz. A simple analysis is carried out to describe the formation of spiral flames from a steady circular flame. © *2008 American Institute of Physics*.
[DOI: 10.1063/1.2836670]

I. INTRODUCTION

Many biological and chemical reaction systems are reported to exhibit spiral wave patterns in the excitable media.[1,2] In chemical systems, the Belousov–Zhabotinsky (BZ) (Ref. 3) reaction medium in liquid phase reactions is one such example which exhibits spiral wave pattern formation. Similar spiral wave patterns have been experimentally observed in premixed,[4] nonpremixed,[5] and solid-phase combustion systems.[6] Premixed gas and solid-phase systems are considerably different from nonpremixed systems due to large heat release rates during combustion and their Arrhenius reaction rate dependence on the temperature of the system. The solid phase combustion systems behave differently from those of gas systems due to a difference in Lewis number, which is infinite for a solid phase combustion system and finite (of order of 1) for the later.[4–6]

It has long been believed that diffusive-thermal imbalance (Lewis number) plays an important role in the excitation of these phenomena for premixed reaction systems. Cellular,[7] radial pulsations,[4] and spiral flames[4,8] are examples of these thermal-diffusive systems. Target pattern flames or radial pulsations (henceforth referred as radial propagation mode) and rotating spiral waves were observed by Pearlman and Ronney[4,8,9] in the near limit mixture of butane and oxygen diluted with helium (Le$\approx$4.0). The formation of these patterns was observed to occur in an exceptionally narrow range of fuel concentration (1.28%–1.50% butane in 21% O_2/He mixture for downward flame propagation at 1 atm pressure and room temperature). Pearlman[9] and Robbins *et al.*[10] also reported the observation of spiral flames with methane-air mixtures on a porous plug burner. In these experiments, the spiral flames were observed for rich methane-air (Le$\approx$1.1), lean propane-air (Le$\approx$1.85), and lean butane-air (Le$\approx$2.08) mixtures.[9] These phenomena were observed for typically very small flow rates (mean flow velocity $\approx$6.4 cm/s) and over a range of mixture equivalence ratios. These spiral flames were observed for a finite time with subsequent transitions to other states, indicating that it was difficult to control these interesting flame behaviors.[11] In this paper, we report the experimental observation of rotating spiral flames in a radial microchannel for a range of mixture flow rates and equivalence ratios. A microchannel for combustion studies is defined as a flow passage whose hydraulic dimensions are smaller than the flame quenching distance ($\leq$2 mm). The spiral flame behaviors observed in these experiments can be controlled by changing the mean wall temperature, mixture equivalence ratio, flow rate, and channel width.

Earlier theoretical studies on spiral dynamics are considered with volumetric replenishment of the reactants over a porous-plug burner.[11,12] Sivashinky[13] applied the linear stability analysis to explain the helical structure of the solid combustion wave. In this model, the helical structure is considered as a pattern resulting from the development of instability and its subsequent nonlinear stabilization. Merzhanov *et al.*[14] have experimentally observed the propagation of a flame front on a thin circular disk composed of solid combustible material which is ignited at the center. The theoretical study by Matkowsky and Volpert[15] on the same case shows that the flame front on the upper surface of the disk propagates at a constant velocity for radii smaller than a critical radius. Once the flame front exceeds the critical size, it becomes unstable and a hot spot appears on the flame front

which follows along an Archimedean spiral. The pattern on the lower surface is the same except for a phase shift. The presence of volumetric fuel source in models[11,12] renders difficulties in their application to the spiral flames observed in radial microchannels. In principle, weak nonlinear approaches will allow us to describe the transition from nonstationary circular to spiral flame, as in the case of premixed methane-air mixtures studied in the present work.

The present work concerns the experimental observation of rotating spiral and radial flame propagation (target pattern) modes in radial microchannels. The interest in microscale combustion devices arises due to major advantages associated with these small-scale systems. Some of these advantages include higher heat and mass transfer coefficients, order of magnitude higher energy densities of hydrocarbon fuels (~20–50 times) compared to electrochemical batteries and lower pollutant emissions, particularly NO_x due to their lower operating temperatures.[16–19] The increased heat loss due to large surface area-volume ratio adversely affects the flame stability limits in these devices. To obtain stable combustion, thermal management, for instance, heat recirculation is a key to enhance the stability limits of these small scale devices. In this technique, the heat is absorbed from exhaust gases in the downstream and transferred to preheat the fresh reactants in the upstream through the solid walls to enhance the combustion stability limits.[16–19] Wall thickness and thermal conductivity play an important role in determining the effective heat recirculation.[17]

Maruta *et al.*[18] have studied the premixed flame propagation characteristics in a 2.0 mm diameter straight quartz tube with a positive wall temperature gradient condition along the flow direction. A steady state wall temperature gradient was applied to channel walls to simplify the target model. This strategy was employed to avoid thermal coupling between the solid and gas phase. This simplification is justifiable if the heat capacity of the solid-phase is much larger (thermally thick) than the gas-phase which is often true for microdevices having microchannels in them. This study showed the existence of various stable and nonstationary flame propagation modes over a range of flow velocities with methane-air mixture. This is a simple, one-dimensional (1D) configuration to study to flame propagation characteristics in the microchannels.

The observation of various unsteady and pulsating modes in a straight channel[18] motivated the authors to investigate and understand these flame instabilities in a simple 2D configuration, such as radial channels. In both configurations (1D and 2D), a positive wall temperature gradient is applied along the flow direction and the channel widths are of same order, about 2 mm. The flow Reynolds number in these configurations varies in the range of 20–500. The initial work on the combustion characteristics of a premixed methane-air mixture in a radial channel configuration is reported in the earlier work[20,21] which was mainly focused on very lean mixtures (at ϕ=0.67) subjected to a positive wall temperature gradient in the direction of flow. These investigations showed that no stable flame propagation modes were observed at ϕ=0.67 for the whole range of mixture flow rates and channel widths. Various nonstationary flame propagation

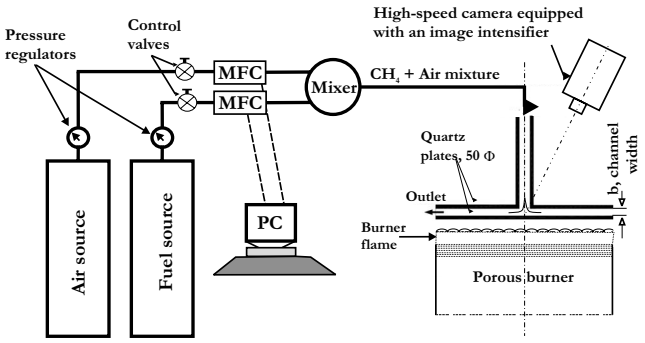

FIG. 1. Details of experimental setup.

modes were observed in which the flame fronts either rotate around the center or travel in the domain of the radial channel. These flame propagation modes were termed as (a) triple flame propagation mode; (b) Pelton flame propagation mode (similar to that of rotating Pelton wheel); (c) traveling flame propagation mode; (d) symmetrical flame propagation mode; (e) unsymmetrical flame propagation mode. The above mentioned names were assigned to these flame propagation modes because of their resemblance to various classical shapes described in the literature.[20,21] Detailed explanations of these flame propagation modes are provided in Refs. 20 and 21. In the present work, the experimental observations on the combustion behavior of methane-air mixtures with their equivalence ratio varying from ϕ=0.85 to 1.25 are presented. These observations show that contrary to flame behavior at ϕ=0.67, a steady circular flame is the dominant mode of combustion at these conditions. Besides the observation of a steady circular flame, rotating spiral and radial propagation modes are observed for slightly lean and rich methane-air mixtures. The characteristics of these rotating spiral and radial propagation modes are distinctly different from the flame modes observed for very lean mixtures. In a real practice, the present work will be helpful in developing a radial microcombustor, where fuel-air mixture is supplied to a configuration such as disk-type combustor for MIT microgas turbine,[22] which is also a similar configuration.

The structure of the present paper is as follows: The details of the experimental setup are described in Sec. II. In Sec. III, a combustion regime diagram for different flame patterns is presented. Experimental observations are also presented in Sec. III. This is followed by a simple theoretical analysis to describe the spiral flame propagation behavior observed in the radial microchannels. Various solutions obtained from this analysis are presented in Sec. IV, followed by conclusions in Sec. V.

II. EXPERIMENTAL SETUP

The schematic diagram of the experimental setup is shown in Fig. 1. Two circular quartz plates are maintained parallel to each other within $\pm 0.1°$ accuracy with the help of a level indicator. To simulate the heat recirculation process with a positive temperature gradient along the flow direction, both quartz plates are heated with the help of a circular cross-section sintered metal burner. This helps in creating a

positive temperature gradient condition in the radial direction, when methane-air mixture is injected at the center through a 4 mm diameter mixture delivery tube. The external heating rate of the porous burner is maintained constant during the experimental investigations to exclude the effect of wall temperature variation with the burner thermal input on the observed flame patterns. The temperature profile along the inner side of the quartz plates in the radial direction is measured in advance with a 300 μm size *K*-type thermocouple. A cooling arrangement is made in a delivery tube to maintain the upstream temperature of the incoming mixture. Methane gas with 99.99% purity is used as fuel during the present investigations. Electric mass flow controllers are used to precisely monitor the mass flow rates of methane (0–1 SLM) and air (0–5 SLM) within $\pm 1\%$ accuracy of the full scale. These mass flow controllers are controlled through a digital to analog converter board connected to a personal computer which enables the independent control of both air and fuel.

Due to the highly unsteady nature of the combustion process, normal movie recording is carried out with the help of a high speed video camera FASTCAM-NEO Photron. High speed video recordings are carried out from an angular position of approximately 30° angle sideways because the presence of the vertical mixture delivery tube restricts the top view of the quartz plates. The resolution of the camera is 512×512 pixels over a range of image capturing speeds varying from 30 Hz to 20000 Hz. This high speed camera is used to observe the flame instabilities at different experimental conditions. Flame images are recorded at a rate of 500 and 1000 frames per second with 1/1000 and 1/2000 s shutter speed, respectively. During each run, 2048 frames are recorded and data is analyzed afterwards. The total runtime depends on the recording speed set for recording the phenomena.

During the beginning of the experiment, a plate separation distance of 5 mm is maintained. The quartz plates are heated with a sintered metal burner and air supply is continued through the mixture delivery tube to obtain the essential condition of a positive wall temperature gradient for present investigations. Once the temperature of plates achieves steady state, fuel supply is initiated along with the continued air supply through the delivery tube. Therefore, methane-air mixture is subjected to a positive temperature gradient and flow divergence through the radial channel. The exhaust gases (high temperature) from the bottom burner ignite the mixture at the outlet of the radial channel and then the flame gradually moves inside the channel. Once the flame is stabilized in the channel, the channel width is reduced by 0.25 mm in each step with the help of a micrometer traverse (0.05 mm resolution).

III. RESULTS AND DISCUSSION

A. Wall temperature profile characteristics

The wall temperature profiles of the top and bottom quartz plates are measured in advance to examine the effects of flow on wall temperature profile. The mixture supply near the center of the plates cools the plates at the center and creates a positive temperature gradient in the flow direction. Figure 2 shows the measured temperature profiles for a thermal input of 1.35 kW from the bottom heating burner and about 3.1% of the total heat was transferred to the incoming reactants through solid walls (approximated from numerical simulations). These temperatures were measured on the inner side of the top and bottom plates for an airflow velocity of 4 m/s (flow rate, $Q \sim 3$ SLM, standard liters per minute) through the delivery tube. The top plate gets heated due to convection and radiation from the bottom plate. Both of these mechanisms play a significant role in the heat transfer between top and bottom plates. The role of convectional heat transfer decreases in the radial direction due to a linear decrease in the Reynolds number, because $\mathrm{Nu} \sim \mathrm{Re}^{1/2}$ and $\mathrm{Re} = \rho^2 U_\infty / 8\mu r$, $\mathrm{Re} \sim r^{-1}$ (where U_∞ is mixture velocity through the mixture delivery tube of diameter d, r is the radial channel distance, ρ is density, and μ is viscosity). Similarly, the role of radiation can also be estimated, which is observed to be quite significant due to high emissivity of quartz glass ($\varepsilon = 0.94-0.96$). Therefore, the measured temperature distribution of both plates is almost similar and the top plate temperature is slightly lower ($\sim 20-50$ K) than the bottom plate. To quantify the effects of mixture velocity on the temperature profile, wall temperature measurements were carried out for a range of velocities varying from 2 to 7 m/s ($Q \sim 1.5-5.25$ SLM) and the bottom plate temperature measurements for a velocity of 2 m/s are shown in Fig. 2. It has been observed that with a decrease in the airflow velocity, the overall temperature profile shrinks, when compared to the temperature profile at 4 m/s. Similarly, an increase in the mixture velocity leads to a widening of the temperature profile. To summarize, the variation in the peak temperature is observed to be less than ± 40 K over a range of mixture velocities for the present experiments (2–7 m/s, $Q \sim 1.5-5.25$ SLM).

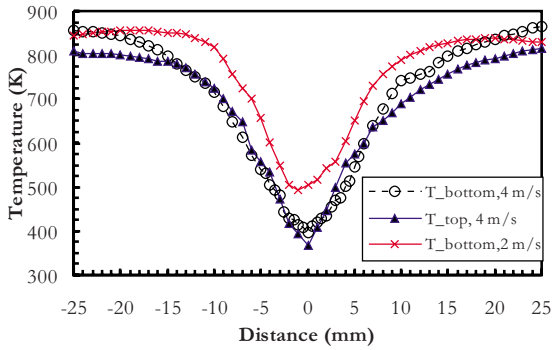

FIG. 2. (Color online) Measured temperature profile of the top and bottom plates at different flow velocities.

B. Combustion regime diagram

Detailed parametric studies are carried out to classify the regions of existence for various stationary and nonstationary flame propagation modes. The flame propagation behavior is recorded with a high speed camera and classified based on

the observed flame front structure. Mixture equivalence ratio, channel width, mixture flow rate and wall temperature profile are important factors which affect shape, size and other characteristics of various flame propagation modes. Mixture equivalence ratio and wall temperature profile are maintained constant to eliminate the variations due to these parameters. Mixture flow rate and channel width are considered as appropriate variables to draw a regime diagram. The regime diagram based on these variables will help understanding the important flame propagation characteristics in the present configuration. The typical mixture velocity through mixture delivery tube (4 mm diameter) is varied in the range of 2–7 m/s ($Q \sim 1.5$–5.25 SLM, $\mathrm{Re} \sim 500$–1800) for the present experiments. The flame gets attached to the mixture delivery tube for smaller velocities (less than 2 m/s, $Q \sim 1.5$ SLM), therefore, it is considered the low velocity limit for present experiments. On the higher side, the present results are limited up to 7 m/s ($Q \sim 5.25$ SLM) mixture velocity because the flow is expected to become turbulent in the mixture delivery tube at ~9 m/s velocity ($Q \sim 6.75$ SLM, $\mathrm{Re} \sim 2300$). Experimental investigations did not show any significant change in the observed flame behavior for 7–9 m/s mixture velocity range ($Q \sim 5.25$–6.75 SLM) except the fact that the flame shifted radially outwards. However, at higher mixture velocities (≥9 m/s), high frequency fluctuations and flickerings akin to turbulent fluctuations were observed when compared to the results in lower flow rate conditions. The role of buoyant forces in the present experiments was assessed through a nondimensional parameter $\mathrm{Gr}/\mathrm{Re}^2$ (ratio of buoyant to conventional forces). The value of this parameter is very small (<0.0001) for the cases investigated in the present experiments. This indicates that buoyant forces do not play any significant role in the present experiments.

Experiments are carried out for a range of equivalence ratios, varying from $\phi = 0.85$ to 1.35 to examine the flame behavior of the premixed mixture subjected to a wall temperature gradient and velocity divergence simultaneously. The behavior of very lean methane-air mixtures ($\phi = 0.67$) leads to a notably different variety of flame pattern formation.[20,21] During the experimental investigations, it has been observed that the regime diagrams at $\phi = 0.85$, 1.0, 1.2, and 1.25 are almost similar (~70%–80% of the diagram) except to the appearance of radial flame propagation mode at lower equivalence ratios and smaller flow rates when compared to the appearance of spiral flame propagation mode at higher equivalence ratios and larger flow rates (>3 SLM). Therefore, only one regime diagram corresponding to $\phi = 1.25$ is presented in this paper, as shown in Fig. 3. The stable flame propagation mode dominates the regime diagram and nonstationary flame propagation modes are observed for intermediate channel widths.

The preliminary experimental investigations showed a strong dependence of plate separation distance and mixture velocity. This leads to the formation of various stationary and nonstationary flame propagation modes and they are classified using the following schemes:

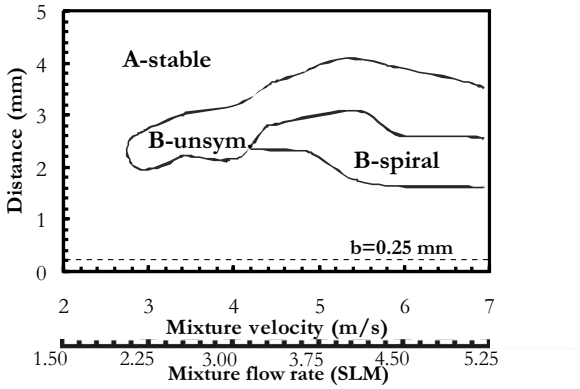

FIG. 3. Regime diagram for different flame propagation modes at $\phi = 1.25$.

(1) Flame propagation modes with stable flame front characteristics are assigned to group A (A-stable).
(2) Flame propagation modes with nonstationary characteristics are assigned to group B (B-unsymmetrical, B-spiral, and B-radial).

Regime A-stable, B-spiral, and B-unsymmetrical dominate in most of the regime diagram. The characteristics of these notable flame patterns observed in rich mixtures are presented in the following sections. The A-stable flame propagation mode dominates the regime diagram as shown in Fig. 3. This hints at the existence of stable combustion over a wide range of operating conditions. For intermediate channel widths ($b = 2.0$–3.5 mm), different nonstationary flame propagation modes like B-spiral and B-unsymmetrical are observed. The low velocity regime is dominated by the presence of A-stable combustion mode. The regime diagrams obtained for $0.85 < \phi < 1.17$ range are similar to that of Fig. 3 for intermediate channel widths ($b \sim 2.0$–3.5 mm) and higher mixture flow rates ($Q > 2.5$ SLM). For intermediate channel widths ($b \sim 2.0$–3.5 mm), radial flame propagation mode appears at intermediate mixture flow rates ($Q \sim 2.0$–3.0 SLM) and low equivalence ratios. A transition from radial propagation mode to spiral propagation mode occurs when mixture equivalence ratio and flow rates are further increased. More details about these flame propagation modes and their transition are provided in the following sections.

C. Visualization of different flame front propagation modes

1. A-stable flame propagation mode

Figure 4 shows a stable flame front named as A-stable which exists over a wide range of operating conditions. This stable flame front is located at a particular radial position. The radial location of this flame front is a function of the mixture velocity and channel width.[23] This mode dominates the combustion regime diagram as shown in Fig. 3. Mixture equivalence ratio also affects the radial position of this stable flame front through a change in burning velocity.

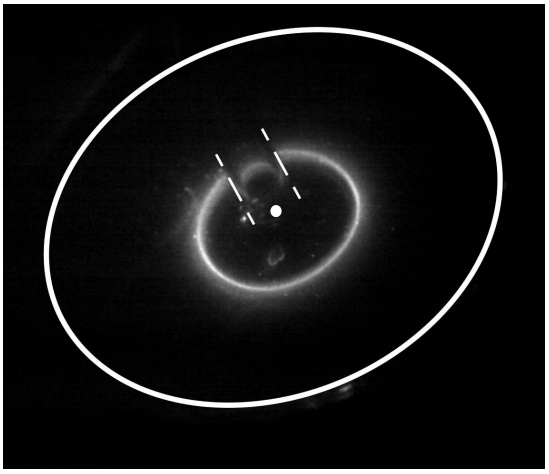

FIG. 4. Flame front propagation in A-stable combustion mode.

2. B-spiral flame propagation mode

Figure 5 shows the evolution and growth of a spiral flame from a circular flame front. These images are recorded at a rate of 500 frames per second and 1/1000 s shutter speed and the captured frames show the flame front position after a time interval of 2 ms. Top plate mixture delivery tube and top plate center are shown with white lines to indicate their respective positions. Since it is difficult to recognize the position of traveling instability and its initial growth owing to its small visual size in still images [shown in Figs. 5(a)–5(c)], two arrows are drawn to indicate its estimated position. This position is determined by playing the high speed video recording (for better understanding of this phenomenon, a supplementary movie is attached with this paper). Under certain conditions of mixture velocity and channel width (as reported in the combustion regime diagram), a small instability appears in the flame front as shown in Figs. 5(a)–5(c). This instability grows into a flame kink (the growth of flame instability at certain points leads to a sudden propagation of a small portion of the flame towards mixture source and this phenomenon is analogous to a sudden and discontinuous decrease in the flame position at a point and henceforth referred as flame kink) over a period of time and travels across the flame front in the angular direction. The simultaneous movement and growth of this flame kink with time is shown in Figs. 5(b)–5(f). At one point of time, a sudden growth of this discontinuous flame front leads to its radially inward movement and it separates from the main flame front. This sequence of inwards movement of the flame kink and separation from the main flame front seems to result in the appearance of partial flame extinction in the domain as seen in Figs. 5(d) and 5(e). This flame kink further grows and finally leads to the formation of a spiral flame propagation mode. This notable change in flame shape occurs over a period of time as shown in Figs. 5(a)–5(f) where the flame develops from a simple circular flame to an intermediary flame kink and finally to a rotating spiral flame.

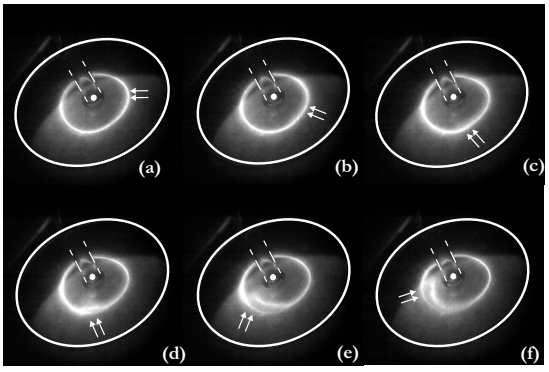

FIG. 5. Development of B-spiral flame propagation mode from a steady A-stable combustion mode. These frames show the flame front position after 2 ms and recorded at a rate of 500 frames per second with 1/1000 s shutter speed. Two arrows are used to indicate the position of the traveling flame instability (enhanced online).

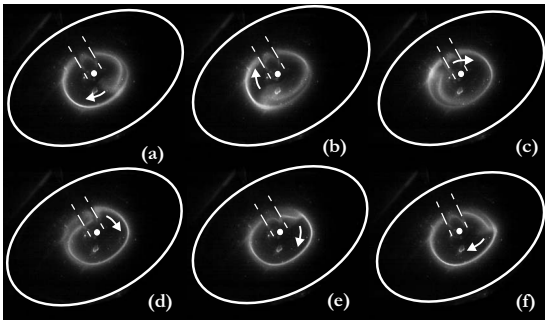

FIG. 6. Flame front propagation in the B-spiral mode. Each frame shows the flame front position after 2 ms time period. $U=5.5$ m/s, $\phi=1.25$ and plate distance, $b=2\pm0.1$ mm (enhanced online).

Figure 6 shows the rotating motion of a spiral flame over a complete cycle. These frames are recorded at a rate of 1000 frames per second and 1/2000 s shutter speed. Each frame shows the position of the propagating flame front after a time interval of 2 ms. These spiral flame movements are recorded at a mixture velocity of 5.5 m/s, $\phi=1.25$, and a plate separation distance of 2 ± 0.1 mm. The typical rotational speed of the propagating spiral flame front shown in Fig. 6 is approximately 83 Hz. The flame tip appears to be slightly thickened, which extends towards to the center. This is followed by a thin and long tail flame with its length greater than 2π angle. The existence of an interface of reactants and combustion products in the domain is perhaps responsible for the long tail of the propagating flame (greater than 2π radial angle) in the present experiments. These engulfed reactants keep burning for a longer time and are responsible for the extension of the flame tail beyond 2π radial length. The flame rotates continuously around the center and tries to move towards the center to achieve a stable state. However, due to adverse conditions (lower wall temperature, higher flow velocity, and smaller residence time near the center), the flame does not stabilize near the center. Hence, the flame continues to rotate in this nonstationary/rotating spiral state at a certain frequency. It has been observed that during this state a decrease in mixture velocity results in the appearance of A-stable flame as shown in Fig. 3 (for mixture velocity ≤ 3 m/s). A

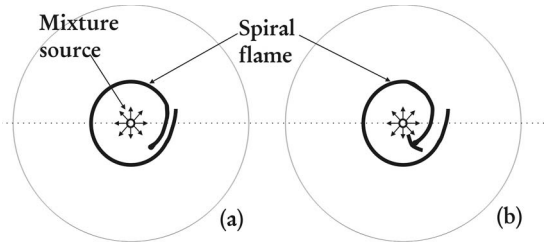

FIG. 7. Line diagram to explain the structure of the rotating spiral flames. (a) Rotating spiral flame corresponding to the flame shown in Fig. 6. (b) Rotating spiral flame corresponding to the flame shown in Fig. 8.

simple hand drawn line diagram is shown in Fig. 7(a) to explain the structure of the rotating spiral flame.

The flame dynamics of these rotating spiral flame fronts was investigated by selecting a point on the tip and tail end of the rotating spiral flame front and these points are tracked for more than ten consecutive and complete cycles. It was observed that the flame tip and tail follow a nearly circular trajectory and this behavior was repeatable for every rotation. The nearly circular motion could be attributed to the symmetric temperature distribution of the channel walls. An asymmetric temperature profile affects the flame trajectory to a certain extent and it changes the flame trajectory to a certain extent.[20,21] However, the flame behavior remains steady as the propagating flame front was observed to follow the same trajectory for consecutive cycles. The rotation of these flames around the center (a periodic motion) remains the dominant mode of flame motion.

Figure 7(b) shows a simple line diagram of a rotating spiral flame observed for a lean mixture condition of $\phi=0.85$. High speed pictures corresponding to this condition are shown in Fig. 8. The flame rotates around the center at a frequency of ~28 Hz, which is smaller than the rotational frequency of the spiral flame at $\phi=1.25$. The flame structure is visibly different from that of the $\phi=1.25$ condition. In this case, the tip of the propagating flame front is much broader, extending from the outer flame towards the mixture source located at the center. A tail originates from the center of this flame and the length of the tail flame is greater than 2π radial length. Although the overall phenomena is similar to the flame propagation mode observed at $\phi=1.25$, the basic difference in the flame shape is possibly due to a change in the equivalence ratio from 0.85 to 1.25 and hence in turn, due to a change in the mixture Lewis number (Le=0.95 for $\phi=0.85$ and 1.11 for $\phi=1.25$). The laminar flame propagation velocity for $\phi=0.85$ and 1.25 mixtures is almost of the same order (~0.32–0.34 m/s).

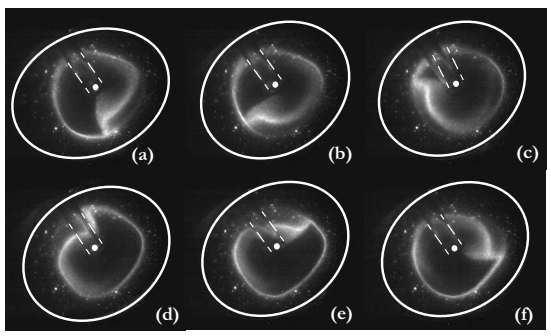

FIG. 8. Spiral flame propagation mode observed at $U=5.5$ m/s, $\phi=0.85$, and plate distance, $b=2\pm0.1$ mm.

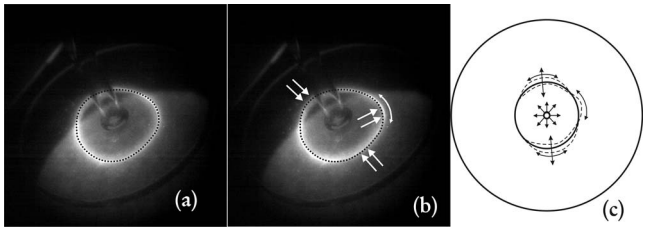

FIG. 9. Oscillation of the flame front in the B-unsymmetrical mode. The pair of arrows is used to indicate the location of the flame front deformation after a time interval of 2 ms.

3. B-unsymmetrical flame propagation mode

Figure 9 shows the direct photographs of the flame fluctuations and a line diagram drawn to describe these fluctuations in B-unsymmetrical mode. In this propagation mode, the symmetry of the flame propagation with respect to the mixture source is broken and it starts randomly oscillating in both angular and radial directions. This mode generally appears during the transition from one A-stable regime to another A-stable regime as the channel width is reduced. For instance, the flame front undergoes through these oscillations as the plate separation distance is reduced for the case of 4 m/s mixture velocity. This is clear from the regime diagram shown in Fig. 3 which shows the presence of a nonstationary combustion zone between two stable combustion zones at ~4 mm and ~1 mm channel width. In this regime, a random instability is generated at a point on the stable flame front with a decrease in the channel width. This instability grows with time and moves across the flame front with a simultaneous decrease in the channel width. In most of the cases, the flame front oscillates at single or multiple locations, about its mean position as shown in Fig. 9. A typical line diagram is shown in Fig. 9(c) to elucidate the actual nature of these oscillations in radial and angular directions.

4. B-radial flame propagation mode

B-radial flame propagation mode is observed to exist for moderately low flow rates ($Q\sim2.25-3.0$) and lean and slightly rich conditions ($0.85<\phi<1.17$) and at intermediate channel widths. Therefore, it is worthwhile to discuss various characteristics of the radial propagation mode in this paper. This will help in understanding the appearance of rotational spiral flames, transition from radial to spiral propagation mode, and overall combustion behavior under various mixture conditions. Figures 10(a)–10(h) show the evolution of a radial flame propagation mode from a circular flame. Figures 10(i)–10(l) show a series of line diagrams drawn to explain the formation of a radial flame propagation mode. The high speed pictures are recorded at a rate of 1000 frames per second and 1/2000 s shutter speed. In this mode, a flame instability moving along the flame surface grows with time

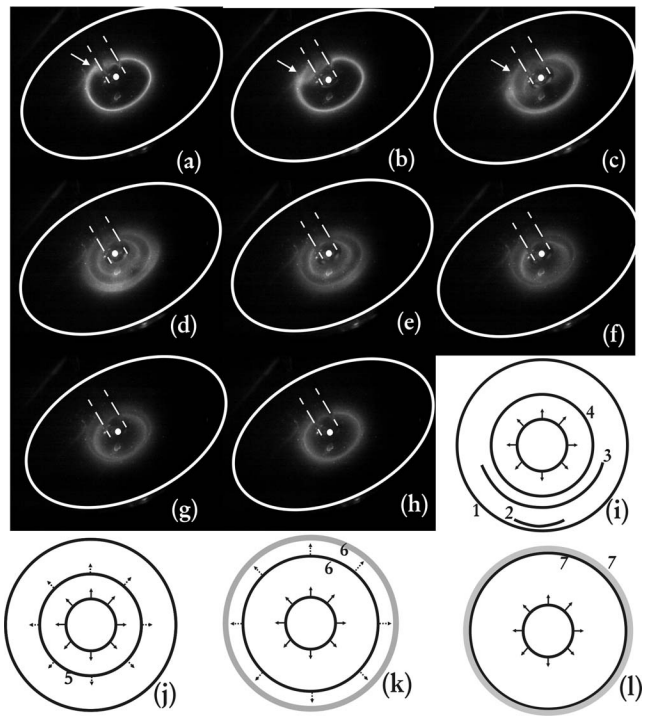

FIG. 10. A radial flame propagation mode. Each frame shows the flame front position after 1 ms time period. $U=5.5$ m/s, $\phi=1.15$, and plate distance, $b=2\pm0.1$ mm (enhanced online).

and develops into a flame kink as seen in Figs. 10(a) and 10(b) (a phenomenon similar to the kink development in spiral flames as discussed in Fig. 5). This flame kink suddenly ignites the mixture closer to the center of the plates and forms a circular ring structure at a smaller radius compared to the original flame location at a larger radius. This is evident from Figs. 10(c) and 10(d) which shows the simultaneous existence of two circular flames at different radial locations. A line drawing in Fig. 10(i) shows the various steps (indicated as 1, 2, 3, and 4) during which a flame kink (2) appears from a circular flame (1) and then subsequently forms a circular flame (4) at a smaller radius. In this position, alternate layers of fresh reactants and combustion products exist at the interface for a very brief time. Due to adverse conditions of high mixture velocity, low residence time and lower wall temperature near the center, the inner circular flame front starts moving outwards as shown by the dotted arrows and steps (5)–(6) in Figs. 10(j) and 10(k). The original flame front at a larger radius weakens with time due to nonavailability of fresh reactants and finally starts disappearing as shown by the fading grey color in steps (6)–(7). The inner circular flame moves outward and merges with the weak outer flame after some time. The outward movement of inner flame and simultaneous weakening/disappearance of the outer flame are shown in Figs. 10(e)–10(h). This whole process described in the preceding lines occurs over a very short time of 8–10 ms. This process repeats after every 30–40 ms.

The radial flame propagation mode is generally observed for moderately low flow rate conditions when compared to that of spiral flames. This mode is observed to occur in $0.85<\phi<1.17$ range of equivalence ratios and spiral flames appear for larger flow rates and extended range of equivalence ratios varying from 0.85 to 1.35. For a given flow rate (moderately low), spiral flame propagation mode is generally observed at strongly rich conditions compared to radial propagation mode ($\phi_{\text{spiral}}>\phi_{\text{radial}}$). For a constant mixture flow rate of ~3 SLM, the transition from radial to spiral propagation mode is observed to occur between $\phi=1.17$ and 1.22.

D. Transition from radial to spiral propagation mode

Present experimental observations show that a transition from radial to spiral flame propagation mode occurs for certain operating conditions of mixture velocity and channel widths with rich methane-air mixtures. A random instability is generated at the flame surface which grows with time and then finally leads to either a radial or a spiral flame propagation mode depending on mixture equivalence ratio. It has been observed that for a mixture flow rate of ~3 SLM, radial mode appears at $\phi=1.17$ or lower and spiral flame propagation mode appears at the same operating conditions of velocity and channel width with $\phi\geq1.25$. It is clear from Figs. 5 and 10 that in these cases, a small disturbance is generated at the flame surface which grows with time and develops into a flame kink. This flame kink finally results in different propagation modes depending on mixture equivalence ratio. This could be due to a decrease in laminar burning velocity of the mixture[24] (by ~15%), when ϕ increases from 1.15 to 1.25. Therefore, at $\phi=1.15$, the random instability generated on the flame surface develops into a flame kink which ignites the mixture at the center due to higher mixture burning velocity and leads to radial flame propagation mode with alternate layers of reactants and combustion products at the interface. At $\phi=1.25$, the flame kink develops into a spiral flame while chasing the fresh methane-air mixture and moving towards the mixture source. The adverse conditions (lower wall temperature, high mixture velocity, and low residence time coupled with lower mixture burning velocity) near the center of the plates prevent further propagation of flame front towards the center.

Various radial and spiral flame propagation modes described in the preceding sections are observed for a range of lean and rich methane-air mixtures. Hydrodynamic, buoyancy-driven, thermal-diffusive (Lewis number) and viscous-fingering are some of the possible mechanisms known for the appearance of flame instabilities in premixed and nonpremixed combustion systems.[25] It is quite possible that Lewis number plays a role in the formation of these behaviors, since the Lewis number for rich methane-air mixtures is slightly greater than 1.0. However, the Lewis number for lean mixtures is slightly less than 1.0 and similar types of pattern formation behaviors are observed with lean methane-air mixtures.[21] The preliminary experiments with lean and rich methane-air (Le~0.95–1.05), lean propane-air (Le~1.83), and lean butane-air (Le~2.13) mixtures show the existence of various flame propagation modes like spiral, radial, and rotating Pelton-type[20,21] flame propagation modes at different equivalence ratios. To summarize, Lewis number

does not explicitly affect the formation of these rotating flame patterns in radial microchannels. A brief summary of these experimental observations with different mixtures is presented in Ref. 21. More experiments are being planned with different fuel-air mixtures to delineate the effect of Lewis number on the formation of these modes. It is more likely that hydrodynamics plays a role in these instabilities due to outward flow which experiences an adverse pressure gradient in the radial microchannel and Reynolds number is of the order of a few hundred at smaller radii and it decreases linearly in the radial direction. We have attempted to explain the primitive mechanism of the propagation and formation of these spiral flames in radial channels. For this, a theoretical analysis based on a constant flame propagation velocity is presented in the next section. Other realistic models for flame burning velocity based on flame curvature, stretch, local concentration and temperature will be considered in the near future for analyzing the overall picture of the phenomenon.

IV. MATHEMATICAL ANALYSIS

The aim of the present analysis is to explain the formation of various flame configurations, such as stable circular flame and rotating spiral flames produced by a radial flow between two closely placed quartz plates and the cylindrical mixture source located at the center. According to the general theory of flammability limits,[26,27] the flame propagation in a narrow channel is impossible if the characteristic distance between channel walls is smaller than a critical value. The condition of flame propagation has the form

$$\mathrm{Pe} = \frac{S_u b}{\alpha_g} \geq \mathrm{Pe}_c, \tag{1}$$

where Pe and Pe_c are the Peclet number and its critical value, b is the channel width, S_u is the burning velocity, and α_g is the thermal diffusivity of the gas. This formula assumes that channel walls have constant temperature, equal to the initial temperature of the unburned mixture. In the case of radial microchannel with temperature gradient, the mixture flowing through the radial channel gets heated and it is assumed that the mixture attains a temperature equal to the solid wall temperature. This assumption appears quite reasonable as the preliminary numerical studies have shown that the difference between the wall and mixture temperature is quite small and it is of the order of 20–50 K. For illustrative purposes, a linear temperature distribution in the radial direction can be defined as

$$T(r) = T_0 + (T_{\max} - T_0)\frac{r - r_o}{R - r_o}, \tag{2}$$

where r is the radius in the polar coordinate, T_0 is mixture temperature at the inner radius r_0, $T_{\max}$ is the maximum wall temperature reached at a disk radius of $r=R$ ($\sim$15 mm). A linear temperature profile $T(r)$ has been assumed because Eq. (2) is the solution of a stationary equation $\Delta T=0$ describing heat conduction in the disks with boundary conditions $T(r_0)=T_0$ and $T(R)=T_{\max}$. Following parameters $T_0=300$ K, $T_{\max}=850$ K, $r_0=2.0$ mm, $R=15$ mm are used in Eq. (2) to approximate the experimental temperature profile (Fig. 2).

A circular flame is stabilized at a point $r=r_f$ where the radial gas velocity $V(r)$ is equal to the local burning velocity, S_u. The unburned mixture flows through the mixture supply tube with a velocity, U, which can be related to the inlet radial gas velocity V_0 in the space between disks by relation $U=2bV_0/r_0$. The $V(r)$ dependency is defined by formula

$$V(r) = \frac{V_0 r_0}{r}\left[\frac{\rho_0}{\rho(r)}\right] = \frac{U r_0^2}{2br}\left[\frac{T(r)}{T_0}\right]. \tag{3}$$

This relation corresponds to a mixture source with intensity $Q=V_0 r_0$ located at the center. The factor $(\rho_0/\rho)=(T/T_0)$ (ρ is the gas density) appears due to the thermal expansion of the gas. The dependence of the burning velocity S_u on the temperature of the unburned mixture entering into the chemical reaction zone can be approximated as[28]

$$S_u(r) = S_{u0}\left[\frac{T(r)}{T_0}\right]^{1.575}, \tag{4}$$

where S_{u0} is burning velocity of the mixture at temperature T_0. Equating $V(r)$ [Eq. (3)] with the expression for local burning velocity $S_u(r)$ [Eq. (4)], an implicit equation defining the flame front position r_f at given U and b can be obtained,

$$r_f\left[\frac{T(r_f)}{T_0}\right]^{0.575} = \frac{U r_0^2}{2bS_{u0}}. \tag{5}$$

When the channel width is less than the critical channel width, the flame can exist in the ring domain indicated by $r_c<r_f<R$, where $r_0<r_c$. The local burning velocity S_u and the thermal diffusivity α_g are functions of mixture temperature and the value of the critical Peclet number Pe_c weakly depends on the temperature of the unburned mixture and to simplify the present analysis it is assumed to be a constant. Thermal diffusivity varies as $\alpha_g=\alpha_{g0}(T(r)/T_0)^{1.6}$, where α_{go} is the thermal diffusivity at temperature T_0, Eq. (1) can be written in the form

$$b \geq b_{0c}\left(\frac{T_0}{T(r_f)}\right)^{0.025}, \tag{6}$$

where $b_{0c}=\alpha_{g0}\mathrm{Pe}_c/S_{u0}$ is the critical channel width corresponding to the unburned mixture with initial temperature T_0. In the case of equality, Eq. (6) yields the value of r_c that defines the minimum radius of the stationary circular flame for a given channel width, b. The minimum gas velocity U_c may be found from the condition of flame stabilization [Eq. (5)] at $r_f=r_c$. On the basis of this criterion, one can obtain the value of minimum velocity for which a flame exists in the radial channel. For a given channel width, b, a cylindrical flame exists if $U\geq U_c$. This velocity limit is given as $U_{\min}=2b_{0c}S_{u0}/r_0$. In this case, the inlet mixture velocity V_0 is equal to S_{u0} and the flame stabilization occurs if $U>U_{\min}$. From this relation, $U_{\min}\approx 0.90$ m/s with $S_{uo}=0.3$ m/s, $b_{oc}=3$ mm, and $r_o=2$ mm. Therefore, flame is expected to exist in the radial channel for mixture velocities higher than 0.9 m/s.

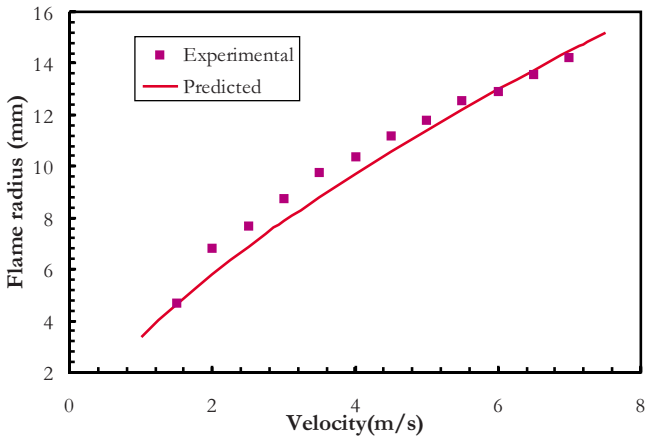

FIG. 11. (Color online) Comparison of the predicted radial flame location with the experimental measurements for stiochiometric CH_4-air mixtures and $b=1.5$ mm.

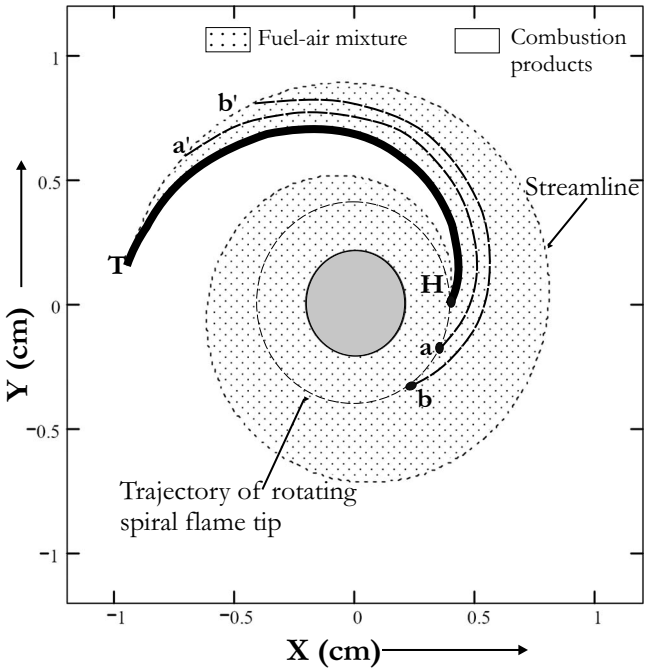

FIG. 12. Convex spiral flame (bold line), interface surface (dashed line) evaluated for $U=1.1$ m/s, $U_{b0}=0.2$ m/s, $r_0=2$ mm, $b=2$ mm, $\omega=521.2$ s^{-1}, and $r_{f0}=4$ mm. $X(=r\cos\varphi)$, $Y=(r\sin\varphi)$ are rectangular coordinates. The shaded circle in the center is the mixture source and the dotted region is the unburned mixture. The flame rotates in the clockwise direction in laboratory coordinates.

Equations (2)–(5) of this model can be used to predict the location of the stabilized circular flame in the radial channel. Figure 11 shows the prediction of the flame location for a stabilized circular flame and these predictions are compared with the experimental measurements[22] for a stoichiometric CH_4-air mixture with $b=1.5$ mm. The predicted flame positions are in reasonably good agreement with the measurements. Therefore, it is clear from this figure that the flame propagation behavior in radial microchannels is governed by the classical flame stabilization mechanisms which states that a flame is stabilized at a location where the local flow velocity equals to the flame propagation velocity.

Various stationary and nonstationary flame propagation modes are observed to exist in the channel width and mixture velocity domain. Spiral flame configuration is one of the propagation modes observed in the experiments. To understand the formation of spiral flames, it is assumed that flame front is a surface which moves along its normal with a velocity S_u, defined by Eq. (4). The radial gas velocity is given by Eq. (3). It is assumed that spiral flame front rotates with constant angular velocity ω in the clockwise direction. For a coordinate frame attached to the rotating flame, the fuel-air mixture moves in the anticlockwise direction relative to the cylindrical coordinates (r,φ) attached to the flame front, where r is radius, and φ is angle. The gas velocity relative to the flame front is given as $\vec{V}=(V(r),\omega r)$. Let us define the flame front by equation $r=f(\varphi)$ and assume that the fresh mixture region is located prior to the combustion products in the radial direction. In this case, $\vec{n}$ is normal to the flame surface, always directed away from combustion products to the fresh mixture and defined as follows:

$$\vec{n}=\left\{-\left[1+\left(\frac{f_\varphi}{f}\right)^2\right]^{-1/2},\frac{f_\varphi}{f}\left[1+\left(\frac{f_\varphi}{f}\right)^2\right]^{-1/2}\right\},$$

where $f_\varphi=\partial f/\partial\varphi$. The condition of flame propagation with velocity S_u leads to the following equation for the flame front:

$$-\vec{V}\cdot\vec{n}=S_u. \tag{7}$$

Equation (7) may be rewritten in the form

$$V(f)f-\omega f f_\varphi=S_u(f)(f^2+f_\varphi^2)^{1/2}. \tag{8}$$

Resolving Eq. (8) with respect to f_φ, one can obtain

$$f_\varphi=\frac{q\Omega f\pm\sqrt{(q\Omega f)^2+(f^2-q^2)(\Omega^2f^2-1)}}{\Omega^2f^2-1}, \tag{9}$$

where $q(f)=fV(f)/S_u(f)$ and $\Omega(f)=\omega/S_u(f)$. This equation admits a trivial solution of $f=q(f)$ and defined by $V(f)=S_u(f)$, that describes a stabilized circular flame near the mixture source. This solution for existence of a stable flame is obtained for a condition $V(f)>S_u(f)$ and no flame exists for the $V(f)<S_u(f)$ condition as described earlier. For positive derivative $f_\varphi>0$ and conditions $\Omega f>1$ and $f>q(f)$ [or $V(f)<S_u(f)$], the solution describing a circular flame does not exist. Assuming that the tangential velocity of the gas is larger than the burning velocity $(\Omega f>1)$, one can see that a positive value on the left-hand side of Eq. (7) leads to a conclusion that the sign before the square root term in Eq. (9) should be negative. The results of the calculation of Eq. (9) are shown in Fig. 12. The equation of the streamline $r=g(\varphi)$ is $gdg=q(g)d\varphi/\Omega(g)$. The solution of this equation with the boundary condition at the flame tip $[g(0)=0.004,\varphi=0]$ determines a curve intersecting with the spiral flame front (see Fig. 12). The solution to this expression is given by $g=\sqrt{1+2q\varphi/\Omega}$. This typical shape is called

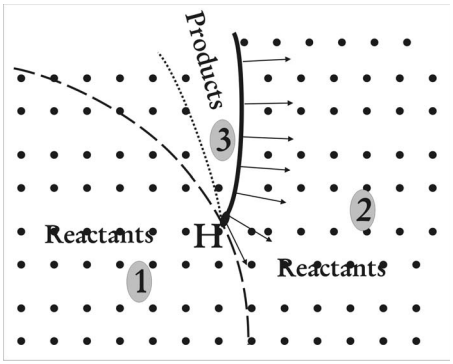

FIG. 13. A zoomed in view of the spiral flame tip.

a convex spiral flame due to its shape with respect to the fuel-air mixture. The intersection point of the streamline with the flame front at its tip and tail determines the maximum possible length of the spiral flame.

To explain the mechanism of the propagation of a spiral flame in a radial channel, additional details are introduced in Fig. 12 and a zoomed view of the flame tip (H) is presented in Fig. 13. These details include the outer dashed circle representing the circular trajectory of flame tip H, and two curves aa′ and bb′. The central shaded circle represents the mixture source. The dotted portion in the domain represents the availability of the fresh fuel-air mixture and nonshaded portion represents the combustion products. A thin dotted streamline which starts from the flame tip (H) and ends at flame tail (T), shows the interface between the reactants (zone 1) and products (represented by zone 3 in Fig. 13). The intersection points of the streamline with the flame tip (H) and tail (T) influence the length of the spiral flame. The spiral flame propagates normally in a direction towards fresh reactants (zone 2) as shown in Fig. 13. Therefore, the flame rotates in clockwise direction as a fresh mixture is available in zone 2 along with favorable conditions (corresponding to local wall temperature, flow rate, and mixture strength) for flame propagation. The flame (denoted by curve HT) propagates into the fresh mixture (in zone 2) and acquires a new position aa′ and then bb′ after certain time intervals. The flame tip (H) does not propagate in the inner direction (towards zone 1) because in zone 1, adverse conditions such as high mixture velocity, low residence time, and low wall temperature does not allow the flame to propagate steadily. Therefore the flame is stabilized at a particular radial location and it rotates around the mixture center. The combustion products get accumulated in zone 3 and an interface is formed between reactants and products. Although the fuel-air mixture in zone 1 is surrounded by an interface of hot combustion products, the mixture does not ignite because of the following reasons. (a) As the combustion products move downstream, due to increased heat loss to the walls, these combustion products get cooled very quickly and thus they are unable to sustain a flame at the interface. (b) A flame propagating into the mixture at the interface would be similar to a concave shaped spiral flame (also shown in Fig. 14) and it will result into an unwinding spiral flame which would finally lead either to a stable circular flame or some other

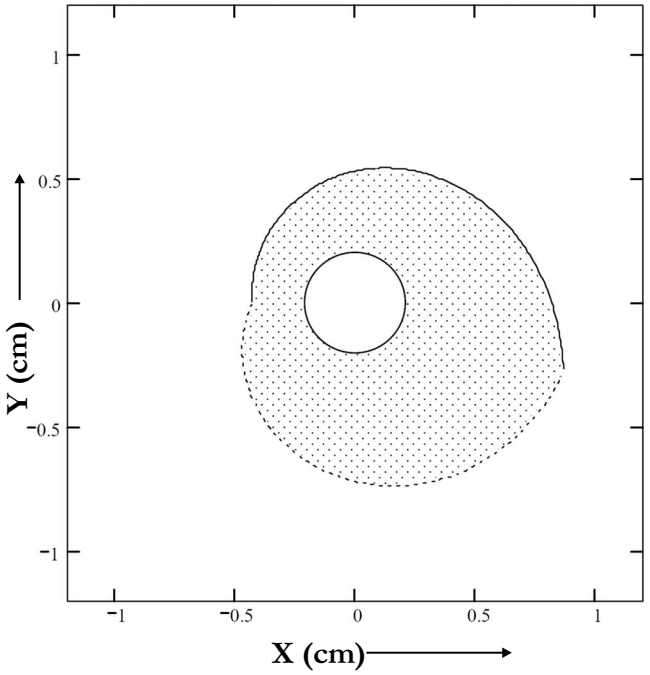

FIG. 14. Concave spiral flame (bold line), interface surface (dashed line) evaluated for $U=1.1$ m/s, $U_{b0}=0.2$ m/s, $r_0=2$ mm, $d=2$ mm, $\omega=188.5$ s^{-1}. The circle in the center is the mixture source and the dotted region is the unburned mixture. The flame rotates in a clockwise direction in laboratory coordinates.

steady flame propagation mode instead of a rotating (convex shaped) spiral flame. The existence of such unwinding spiral flame configurations has not been reported in the literature.

Equation (9) also admits another solution corresponding to a condition of $f_\phi<0$ which describes a spiral flame with a concave shape (defined with respect to the fuel-air mixture) as shown in Fig. 14. It is quite difficult to experimentally observe such spiral flame shape because the flame front always propagates in a direction normal to the flame surface, pointing towards the reactants. Therefore, in a concave spiral flame case, the flame will perhaps consume the mixture and revert back to a more stable configuration such as a circular flame.

The present analysis has helped in understanding some of the important features like formation and propagation mechanisms of a spiral and stable circular flames which resemble those observed in the experiments. The "B-spiral" and the "A-stable" flame modes may be considered as two basic combustion modes. The loss of stability and further nonlinear stabilization of primarily circular flame shape may lead to the formation of either stationary cracks or local oscillations at the circular flame front. The periodical bending of the circular flame or local oscillations in the flame front like those in the "B-unsymmetrical mode" (Fig. 9) case may also be attributed to the nonstationary circular flame. These phenomena may be captured within the frame of future nonstationary thermal-diffusive models.

V. CONCLUSIONS

The present study reports the experimental observation of radial and spiral flame propagation modes with lean, stoi-

chiometric and rich methane-air mixtures in radial microchannels in which the mixture is subjected to a positive wall temperature gradient. Radial and quasisteady spiral flame propagation modes are observed over a range of mixture velocities and channel widths. A radial propagation mode is observed at $\phi=0.85-1.17$ and at moderately lower flow rates and spiral propagation mode is observed at $\phi=0.85-1.35$ and comparatively higher flow rates. Radial to spiral flame transition for methane-air mixtures occurs over a range of mixture equivalence ratio, varying from 1.17 to 1.22. A simple analysis is introduced to explain the propagation mechanism of spiral and steady circular flames. It shows that the presence of an interface of fresh reactants and combustion products results in a long tail of spiral flames as observed in the present experiments. Similar interface of combustion products and reactants also exists for the radial flame propagation mode, which is responsible for the appearance of multiple flames at different radial locations.

ACKNOWLEDGMENTS

The authors would like to thank Professor S. Maruyama, IFS and Professor Paul Ronney of USC for having useful, interesting, and thought-provoking discussions while carrying out this work. The authors would also like to thank Mr. S. Hasegawa for help in the experimental setup and useful suggestions for conducting the present experiments.

[1] J. M. Davidenko, A. V. Pertsov, R. Salomonsz, W. Baxter, and J. Jalife, "Stationary and drifting spiral waves of excitation in isolated cardiac muscle," Nature (London) **355**, 349 (1992).
[2] D. Murray, *Mathematical Biology* (Springer, Berlin, 1993).
[3] A. N. Zaikin and A. M. Zhabotinsky, "Concentration wave propagation in two-dimensional liquid-phase self-oscillating system," Nature (London) **225**, 535 (1970).
[4] H. G. Pearlman and P. D. Ronney, "Self-organized spiral and circular waves in premixed gas flames," J. Chem. Phys. **101**, 2632 (1994).
[5] V. Nayagam and F. A. Williams, "Rotating spiral edge flames in von Karman swirling flows," Phys. Rev. Lett. **84**, 479 (2000).
[6] A. G. Merzhanov, "Solid flames: Discovery, concepts and horizons of cognition," Combust. Sci. Technol. **98**, 307 (1994).
[7] M. el Hamdi, M. Gorman, and K. Robbins, "Deterministic chaos in laminar premixed flames: Experimental classification of chaotic dynamics," Combust. Sci. Technol. **94**, 87 (1993).
[8] H. G. Pearlman and P. D. Ronney, "Near-limit behavior of high-Lewis number premixed flames in tubes at normal and low gravity," Phys. Fluids **6**, 4009 (1994).
[9] H. Pearlman, "Excitability in high-Lewis number premixed gas combustion," Combust. Flame **109**, 382 (1997).
[10] K. Robbins, M. Gorman, J. Bowers, and R. Brockman, "Spiral dynamics of pulsating methane-oxygen flames on a circular burner," Chaos **14**, 467 (2004).
[11] S. K. Scott, J. Wang, and K. Showalter, "Modelling studies of spiral waves and target patterns in premixed flames," J. Chem. Soc., Faraday Trans. **93**, 1733 (1997).
[12] V. Panfilov, A. Bayliss, and B. J. Matkowsky, "Spiral flames," Appl. Math. Lett. **16**, 131 (2003).
[13] G. Sivashinsky, "On spinning propagation of combustion waves," SIAM J. Appl. Math. **40**, 432 (1981).
[14] A. G. Merzhanov, A. V. Dvoryankin, and A. G. Strunina, "New type of spin burning," Dokl. Phys. Chem. **267**, 869 (1982).
[15] B. J. Matkowsky and V. Volpert, "Spiral gasless condensed phase combustion," SIAM J. Appl. Math. **541**, 132 (1994).
[16] A. C. Fernadez-Pello, "Micro power generation using combustion: Issues and approaches," Proc. Combust. Inst. **29**, 883 (2002).
[17] P. D. Ronney, "Analysis of nonadiabatic heat-recirculating combustors," Combust. Flame **135**, 421 (2003).
[18] K. Maruta, T. Kataoka, N. I. Kim, S. Minaev, and R. Fursenko, "Characteristics of combustion in a narrow channel with a temperature gradient," Proc. Combust. Inst. **30**, 2429 (2005).
[19] S. A. Lloyd and F. J. Weinberg, "A burner for mixtures of very low heat content," Nature (London) **251**, 47 (1974).
[20] S. Kumar, K. Maruta, and S. Minaev, "On the formation of multiple rotating Pelton-like flame structures in radial microchannels with lean methane-air mixtures," Proc. Combust. Inst. **31**, 3261 (2007).
[21] S. Kumar, K. Maruta, and S. Minaev, "Pattern formation of flames in radial microchannel with lean methane-air mixtures," Phys. Rev. E **75**, 016208 (2007).
[22] A. H. Epstein, S. D. Senturia, G. Anathasuresh, A. Ayon, K. Breuer, K.-S. Chen, F. Ehrich, G. Gauba, R. Ghodssi, C. Groshenry, S. Jacobson, J. Lang, C.-C. Mehra, J. Mur Miranda, S. Nagle, D. Orr, E. Piekos, M. Schmidt, G. Shirley, S. Spearing, C. Tan, Y.-S. Tzeng, and I. Waitz, "Power MEMS and microengines," *Proceedings of International Solid State Sensors and Actuators Conference (Transducers '97)*, 16–19 June 1997, Chicago, IL (IEEE, New York, 1997), Vol. 2, p. 753.
[23] S. Kumar, K. Maruta, and S. Minaev, "Experimental investigations on the combustion behavior of methane-air mixtures in a micro-scale radial combustor configuration," J. Micromech. Microeng. **17**, 900 (2007).
[24] S. R. Turns, *An Introduction to Combustion* (McGraw-Hill, Singapore, 1996), p. 228.
[25] F. A. Williams, *Combustion Theory* (Benjamin Cummings, Menlo Park, 1985), p. 341.
[26] Ya. B. Zel'dovich, "Theory of the propagation limit of a quiet flame," Zh. Eksp. Teor. Fiz. **11**, 159 (1941).
[27] D. B. Spalding, "A theory of inflammability limits and flame-quenching," Proc. R. Soc. London, Ser. A **240**, 83 (1957).
[28] D. P. Mishra, "Effects of initial temperature on the structure of laminar CH_4-air premixed flames," Fuel **82**, 1471 (2003).